European Journal of Control 19 (2013) 266–278

Contents lists available at SciVerse ScienceDirect

European Journal of Control

journal homepage: www.elsevier.com/locate/ejcon

Adaptive regulation via weighted robust estimation and automatic controller tuning

Raymond A. de Callafon [a,*], Huazhen Fang [b]

[a] Faculty of Mechanical and Aerospace Engineering, University of California San Diego, 9500 Gilman Drive, Mail Code 0411, La Jolla, CA 92093-0411, USA
[b] Department of Mechanical and Aerospace Engineering, University of California San Diego, 9500 Gilman Drive, Mail Code 0411, La Jolla, CA 92093-0411, USA

ARTICLE INFO

Article history:
Received 6 February 2013
Accepted 3 May 2013
Recommended by I.D. Landau/D.W. Clarke
Available online 9 May 2013

Keywords:
Adaptive regulation
Recursive estimation
Uncertain systems
Vibration control

ABSTRACT

This paper proposes a methodology to adaptively reduce time-varying additive disturbances in a feedback system, comprised a plant with uncertainty and an adaptable linear feedback controller. Adaptive regulation is done via the direct estimation of a perturbation on the feedback controller in a Youla–Kucera parametrization. Uncertainty on the plant dynamics bounds the size of the allowable controller perturbation for adaptation to maintain stability robustness. By simultaneously minimizing the variance of the plant output signal and a control output signal, the direct estimation of the controller perturbation is formulated as a weighted robust estimation problem that is implemented recursively for a real-time implementation. The methodology is applied to a vibration control benchmark to demonstrate how the proposed adaptive feedback regulation can effectively reduce unknown harmonic disturbances with a time-varying frequency for a mechanical system with unmodelled dynamics.

1. Introduction

Feedback control can be effective in reducing the effect of unknown additive plant output disturbances. The more information is known on the disturbance dynamics, the better the feedback control algorithm can be tuned to alleviate the effects of the disturbances. A good example is the internal model principle [9] or the more general form of repetitive control [25,23] that use resonators in the feedback controller to compensate for general periodic disturbances. Feedback compensation of periodic disturbances also can be shown to be equivalent to adaptive feedforward compensation [2] under certain conditions. The requirements on maintaining closed-loop stability in feedback control require knowledge on the plant dynamics [21], whereas fixed linear feedback control imposes limitations on the frequency range over which disturbances can be reduced.

Limitations of fixed linear feedback control are well captured by the celebrated Bode Sensitivity integral [27,22,20]

$$\int_0^\infty \ln|S(j\omega)|\, d\omega = -\frac{\pi}{2}\lim_{s\to\infty} sL(s)$$

for a feedback connection

$$y = Gu + v, \quad v = He$$
$$u = C(r-y) \tag{1}$$

of a stable system G and stable controller C with a loop gain $L(s) = G(s)C(s)$ and a sensitivity function $S(s) = (1 + L(s))^{-1}$. A challenging problem arises when the spectral contents of the disturbance, modelled by H in (1), changes over time. Changes in disturbance dynamics H may result in amplification of the disturbance $v(t)$ in (1) due to a gain $|S(j\omega)| > 1$ of the sensitivity function. Adaptive solutions for this problem have been proposed using feedforward control [8] that rely on linearly parametrized filters with recursive estimation techniques [6], but require additional sensors for measuring or estimating the disturbance v.

Adaptive regulation [15] is a viable solution to deal with varying disturbance dynamics in feedback control. Adaptive regulation has been studied for periodic disturbances [3,2] and with Iterative Learning Control (ILC) [18,5,24]. With knowledge of the (stable) plant dynamics G, the disturbance v could be reconstructed via $v = y - Gu$, using plant input u and output y signals, leading to a new class of algorithms based on filtered white noise disturbances in [15]. More recently, the ideas of adaptive regulation have been extended to specific classes of periodic disturbances [16]. Earlier work of Robust Estimation and Automatic Controller Tuning (REACT) [12] demonstrated how such algorithms can be implemented in real-time but did not explicitly take into account the variance of the control signal during adaptation. As minimum variance control can lead to large control signals, especially for non-minimum phase systems [1], it is clear that optimizing the performance of a controller in adaptive regulation must minimize the variance of a plant output signal *y and* a control output signal u.

The resulting *weighted REACT approach* proposed in this paper allows a trade-off between minimizing output y variance to reduce time varying disturbances, weighted against the variance of the

* Corresponding author. Tel.: +1 858 534 3166; fax: +1 858 822 3107.
E-mail addresses: callafon@ucsd.edu (R.A. de Callafon), hufang@ucsd.edu (H. Fang).

0947-3580/$ - see front matter © 2013 European Control Association. Published by Elsevier Ltd. All rights reserved.
http://dx.doi.org/10.1016/j.ejcon.2013.05.009

control signal u. It is shown in this paper that the resulting weighted controller adaptive regulation can be formulated as a Recursive Least Squares minimization problem in which the feedback controller transfer function is parametrized in a Youla–Kucera parametrization. The use of coprime factorization in the Youla–Kucera parametrization allows for adaptive regulation for both stable and unstable plants and controller dynamics, whereas the proper choice of coprime factorization enables well-defined filtering properties of plant input u and output y signals to reconstruct a (filtered) disturbance v for adaptive regulation.

The weighted REACT approach is applied to a vibration control benchmark to demonstrate how the proposed adaptive feedback regulation can effectively reduce unknown harmonic disturbances. Plant uncertainty is taken into account by including a frequency weighting on the control energy. It is shown that a single adaptive regulation algorithm can handle a wide class of time-varying harmonic disturbances with excellent disturbance rejection properties.

2. Adaptive regulation via recursive convex optimization

2.1. Controller parametrization

A well-known result in controller design and optimization is the Youla–Kucera parametrization [1] that allows the parametrization of the class of all stabilizing feedback controllers C for a given dynamical system G by a single stable dynamical perturbation Q. The parametrization can be formulated in terms of a right coprime factorization (rcf) of a model $\hat{G}$ and an initial stabilizing feedback controller C_i. Defining the closed-loop transfer functions

$$T(C,G)=\begin{bmatrix} C \\ I \end{bmatrix}(I+GC)^{-1}[G\ \ I]$$

the Youla–Kucera parametrization is as follows.

Definition 1. Youla–Kucera parametrization. Consider the feedback connection of a nominal model $\hat{G}$ and an initial controller C_i with $T(C_i,\hat{G})\in\mathcal{RH}_\infty$. All $C_Q=N_QD_Q^{-1}$ that satisfy $T(C_Q,\hat{G})\in\mathcal{RH}_\infty$ are given by the rcf

$$\begin{matrix} N_Q=N_i+DQ \\ D_Q=D_i-NQ \end{matrix},\quad Q\in\mathcal{RH}_\infty$$

where (N,D) is a rcf of $\hat{G}$ and (N_i,D_i) is a rcf of C_i.

A similar definition can also be given for a left coprime factorization (lcf) $(\tilde{N},\tilde{D})$ of $\hat{G}$. The coprime factorization can be used to formulate internal stability of a feedback connection of C and G [27] as $T(C,G)\in\mathcal{RH}_\infty$ for internal stability is equivalent to $\Lambda^{-1}\in\mathcal{RH}_\infty$, with $\Lambda=\tilde{D}D_c+\tilde{N}N_c$. It is also a well-known result that the Youla–Kucera parameter Q can be varied to find new controllers for the nominal model $\hat{G}$. As long as $Q\in\mathcal{RH}_\infty$, stability can be maintained for the feedback of C_Q and $\hat{G}$.

For a known (optimal) controller C_Q, the stable Youla–Kucera parameter Q can be computed explicitly via $Q=D^{-1}(I+C_Q\hat{G})^{-1}[C_Q-C_i]D_i$, where coprime factors N,D and (N_i,D_i) can be computed via standard state feedback solutions [27]. With a stable model $\hat{G}$, a trivial choice is obtained for the rcf with $N=\hat{G}$, $D=I$ for $\hat{G}$, while $N_i=C_i$, $D_i=I$ for a stable initial controller C_i. In that case, the adapted controller C_Q will simplify to

$$C_Q=(C_i+Q)(I-\hat{G}Q)^{-1} \tag{2}$$

where Q must again satisfy $Q\in\mathcal{RH}_\infty$ due to the Youla–Kucera parametrization.

2.2. Mixed performance and control optimization

Next to providing a parametrization of all stabilizing controllers, the Youla–Kucera parametrization in Definition 1 provides an another advantage for controller adaptation: all closed-loop transfer functions are linear in the Youla–Kucera parameter Q. Considering a feedback system

$$\begin{aligned} y(t)&=\hat{G}u(t)+He(t) \\ u(t)&=-C_Qy(t) \end{aligned} \tag{3}$$

the weighted REACT approach in this paper aims at minimizing the weighted two-norm performance measure

$$\left\| \begin{matrix} \gamma u_w \\ y \end{matrix} \right\|_2,\quad u_w(t)=W(q)u(t) \tag{4}$$

that measures the combined variance of the performance signal $y(t)$ and a filtered control signal u given in (3). The filter $W(q)$ is a user-specified monic stable filter. Monicity of $W(q)$ allows an additional scalar weighting γ in the weighted two-norm performance measure of (4).

The variance of $y(t)$ and $u(t)$ is driven by the noise disturbance $v(t)=H(q)e(t)$, where $e(t)$ is a white noise signal with a variance ν and $\Phi_v(\omega)=|H(e^{j\omega})|^2\nu$ would be an unknown and possibly time varying spectrum of the noise disturbance. The Youla–Kucera parametrization in Definition 1 allows the weighted two-norm performance measure of (4) to be written as an affine function of the stable Youla–Kucera parameter Q. The result is summarized in the following corollary.

Corollary 1. *Consider a nominal model $\hat{G}$ and an initial controller C_i with $T(C_i,\hat{G})\in\mathcal{RH}_\infty$. A controller C_Q parametrized according to Definition 1 that minimizes (4) can be computed by*

$$\min_{Q\in\mathcal{RH}_\infty}\|W_1M_{22}W_2+W_1M_{21}QM_{12}W_2\|_2$$

where

$$\begin{aligned} M_{22}&=\begin{bmatrix} N_i \\ D_i \end{bmatrix}\Lambda_i^{-1}[\tilde{N}\ \ \tilde{D}]=T(C_i,\hat{G}) \\ M_{21}&=\begin{bmatrix} D \\ -N \end{bmatrix} \\ M_{12}&=\Lambda_i^{-1}[\tilde{N}\ \ \tilde{D}]=D_i^{-1}(I+C_i\hat{G})^{-1}[\hat{G}\ \ I] \\ W_1&=\begin{bmatrix} -\gamma W & 0 \\ 0 & I \end{bmatrix},\quad W_2=\begin{bmatrix} 0 \\ H \end{bmatrix} \end{aligned}$$

and $\Lambda_i=\tilde{D}D_i+\tilde{N}N_i\in\mathcal{RH}_\infty$.

The proof of Corollary 1 is straightforward by recognizing that $\Lambda_i=\tilde{D}D_i+\tilde{N}N_i\in\mathcal{RH}_\infty$ and $T(C_Q,\hat{G})$ can be rewritten as

$$\begin{bmatrix} N_i \\ D_i \end{bmatrix}\Lambda_i^{-1}[\tilde{N}\ \ \tilde{D}]+\begin{bmatrix} D \\ -N \end{bmatrix}Q\Lambda_i^{-1}[\tilde{N}\ \ \tilde{D}]$$

so the map from $e(t)$ to $[u_w(t)\ y(t)]^T$ is given by $W_1T(C_Q,\hat{G})W_2$. The affine relation in Q for the minimization of (4) will be exploited in a (Recursive) Least Squares closed-loop data-based solution in the weighted REACT algorithm.

2.3. Closed-loop data-based minimization

A data-based solution for minimizing the combined variance of the performance signal $y(t)$ and a filtered control signal $u_w(t)=W(q)u(t)$ given in (3) can be formulated based on the closed-loop data obtained from the feedback system. To enable a data-based solution, we first write $y(t)$ and $u_w(t)$ as an affine function of Q in the following result.

Corollary 2. *Consider a nominal model $\hat{G}$ with a rcf (N,D), an initial controller C_i with a rcf (N_i,D_i) and $T(C_i,\hat{G})\in\mathcal{RH}_\infty$. If a controller C_Q is parametrized according to Definition*1, *then*

$$\begin{bmatrix}\gamma u_w(t)\\ y(t)\end{bmatrix}=\begin{bmatrix}-\gamma WN_i\\ D_i\end{bmatrix}w(t)-\begin{bmatrix}\gamma WD\\ N\end{bmatrix}Qw(t) \tag{5}$$

where

$$w(t)=\Lambda_i^{-1}[\tilde{N}\ \ \tilde{D}]\begin{bmatrix}-u(t)\\ y(t)\end{bmatrix} \tag{6}$$

is a filtered closed-loop signal.

The proof of this result is found by first writing $y(t)=\hat{G}u(t)+v(t)$, where $\hat{G}=\tilde{D}^{-1}\tilde{N}$ as $\tilde{D}y(t)=\tilde{N}u(t)+\tilde{D}v(t)$. With $v(t)=He(t)$, the filtered output noise $\Lambda_i^{-1}\tilde{D}v(t)$ can be written as

$$\Lambda_i^{-1}\tilde{D}He(t)=\Lambda_i^{-1}\tilde{D}y(t)-\Lambda_i^{-1}\tilde{N}u(t)$$

Based on this analysis, the filtered closed-loop signal $w(t)$ in (6) can be defined and it should be noted that $w(t)$ is bounded, as $\Lambda_i^{-1}\in\mathcal{RH}_\infty$ with $T(C_i,\hat{G})\in\mathcal{RH}_\infty$ and obviously $(\tilde{D},\tilde{N})\in\mathcal{RH}_\infty$. Using the affine relation in the Youla–Kucera parameter Q summarized in Corollary 1 allows us to write

$$\begin{bmatrix}\gamma u_w(t)\\ y(t)\end{bmatrix}=\left(\begin{bmatrix}-\gamma WN_i\\ D_i\end{bmatrix}-\begin{bmatrix}\gamma WD\\ N\end{bmatrix}Q\right)\Lambda_i^{-1}\tilde{D}He(t)$$

creating the result in (5).

The signal $w(t)=\Lambda_i^{-1}\tilde{D}He(t)$ in (6) basically reconstructs a (closed-loop filtered) disturbance signal $v(t)=He(t)$ via the closed-loop signals $u(t)$ and $y(t)$. It can be noted here that the use of coprime factorizations and the knowledge of a stabilizing initial controller C_i makes the signal $w(t)$ more general than an output or equation error observer of the disturbance signal $v(t)$. In the case $\hat{G}$ is stable, one could select $C_i=0$ as an initial controller. With the trivial choices for the coprime factorization $(N_i,D_i)=(0,I)$ for $C_i=0$ we see that $\Lambda_i=\tilde{D}D_i+\tilde{N}N_i=\tilde{D}$ and the expression for $w(t)$ reduces to the output error $w(t)=y(t)-\hat{G}u(t)$, irrespective of the coprime factorization $(\tilde{D},\tilde{N})$ of $\hat{G}$. Choosing a non-zero, but stable controller C_i with the trivial choice $(N_i,D_i)=(C_i,I)$ for the coprime factorization of C_i and a trivial coprime factorization $(\tilde{D},\tilde{N})=(I,\hat{G})$ of a stable $\hat{G}$ will lead to $\Lambda_i=\tilde{D}D_i+\tilde{N}N_i=(I+\hat{G}C_i)$. This leads to a more familiar expression for $w(t)=(I+\hat{G}C_i)^{-1}y(t)-(I+\hat{G}C_i)^{-1}\hat{G}u(t)$ in which we can recognize the sensitivity function $(I+\hat{G}C_i)^{-1}$, making $w(t)=\Lambda_i^{-1}\tilde{D}He(t)=(I+\hat{G}C_i)^{-1}He(t)$ a closed-loop filtered disturbance signal. The additional freedom in the choice of coprime factorizations can be exploited to influence the scaling and filtering of the signal $w(t)$.

By allowing a parametrization of $Q(\theta)$, the error signal

$$\varepsilon(t,\theta)=\begin{bmatrix}-\gamma WN_i\\ D_i\end{bmatrix}w(t)-\begin{bmatrix}\gamma WD\\ N\end{bmatrix}Q(\theta)w(t) \tag{7}$$

will be linear in the parameter θ if and only if $Q(\theta)\in\mathcal{RH}_\infty$ is parameterized linearly in the parameter θ. An obvious choice for $Q(\theta)\in\mathcal{RH}_\infty\forall\theta$ that is parametrized linearly in θ would be a (finite dimensional) FIR model

$$Q(q,\theta)=b_0+\sum_{k=0}^{\bar{k}-1}b_{k+1}q^{-k-1},\quad \theta=[b_0\ b_1\ \cdots\ b_{\bar{k}}]^T \tag{8}$$

of order $\bar{k}$. This parameterization of $Q(q,\theta)$ allows a convex optimization of (4) over θ due to the fact that

$$\begin{aligned}\left\|\begin{matrix}\gamma u_w\\ y\end{matrix}\right\|_2&=\lim_{N\to\infty}\frac{1}{N}\sum_{t=1}^{N}\varepsilon(t,\theta)^T\varepsilon(t,\theta)\\&=\left\|\begin{bmatrix}-\gamma WN_i\\ D_i\end{bmatrix}w(t)-\begin{bmatrix}\gamma WD\\ N\end{bmatrix}Q(\theta)w(t)\right\|_2\end{aligned} \tag{9}$$

using Parseval's theorem [17]. In conclusion, a closed-loop data-based convex optimization of the parameter θ in the controller perturbation $Q(q,\theta)$ can be formulated, with $\varepsilon(t,\theta)$ given in (7) and depending solely on the filtered closed-loop signal $w(t)$ given in (6) and the known rcf (N_i,D_i) of the initial controller C_i and the known rcf (N,D) of the nominal model $\hat{G}$.

Finally, it should be noted that the parametrization of $Q(q,\theta)$ in (8) will not limit the shape and size of $|Q(e^{j\omega},\theta)|$, possibly leading to a high frequency gain due to the freedom in the FIR filter. The parametrization of $Q(q,\theta)$ can be extended with a fixed stable denominator to allow for additional filtering and limit the control to a specific frequency range. Additionally, with information on desirable pole locations for $Q(q,\theta)$, a parametrization using rational orthogonal basis function [11] can be used, as linearity and stability are preserved. In this paper we left these options open and assumed no information on desirable frequency range and/or pole locations in $Q(q,\theta)$.

2.4. Recursive solutions

To anticipate changes in the spectrum $\Phi_v(\omega)$, the combined variance of the performance signal $y(t)$ and a filtered control signal $u_w(t)$ is computed only over a finite number of time samples. The finite time computation is used to formulate a Recursive Least Squares (RLS) solution.

For a Single Input Single Output (SISO) system (with $\tilde{D}=D$ and $\tilde{N}=N$) the expression of the error signal in (7) can be simplified to $\varepsilon(t,\theta)=y_f(t)-\mathrm{diag}\{Q(\theta)\}u_f(t)$ where $Q(\theta)$ is now a *scalar* FIR transfer function as in (8) and

$$\mathrm{diag}\{Q(\theta)\}=\begin{bmatrix}Q(\theta)&0\\ 0&Q(\theta)\end{bmatrix}$$

and $y_f(t)$ denotes the filtered output and $u_f(t)$ denotes the filtered input signals

$$\begin{aligned}&y_f(t)=\begin{bmatrix}-\gamma WN_i\\ D_i\end{bmatrix}w(t),\quad u_f(t)=\begin{bmatrix}\gamma WD\\ N\end{bmatrix}w(t)\\&w(t)=\frac{D}{\Lambda_i}y(t)-\frac{N}{\Lambda_i}u(t)\end{aligned} \tag{10}$$

To formulate a recursive solution for the minimization

$$\begin{aligned}&\hat{\theta}_t=\min_\theta\frac{1}{t}\sum_{\tau=0}^{t}\varepsilon(\tau,\theta)^T\varepsilon(\tau,\theta),\\&\varepsilon(t,\theta)=y_f(t)-\mathrm{diag}\{Q(\theta)\}u_f(t)\end{aligned} \tag{11}$$

for a linearly parametrized scalar $Q(q,\theta)$, the error $\varepsilon(t,\theta)$ can be written in a linear regression form

$$\begin{aligned}&\varepsilon(t,\theta)=y_f(t)-\phi(t)^T\theta\in\mathcal{R}_{2\times1}\quad\text{with}\\&\phi(t)^T=[u_f(t)\ u_f(t-1)\ \cdots\ u_f(t-\bar{k})]\in\mathcal{R}_{2\times\bar{k}+1}\\&\theta=[b_0\ b_1\ \cdots\ b_{\bar{k}}]^T\in\mathcal{R}_{\bar{k}+1\times1}\end{aligned}$$

where the regressor $\phi(t)$ contains past and/or filtered versions of the input signal $u_f(t)$.

A standard RLS update algorithm [17,10] can be summarized by the three iterative steps of an *a posteriori* prediction error update

$$\varepsilon(t,\hat{\theta}_{t-1})=y(t)-\phi(t)^T\hat{\theta}_{t-1} \tag{12}$$

a time weighted covariance update

$$P_t=P_{t-1}-P_{t-1}\phi(t)[\phi(t)^TP_{t-1}\phi(t)+I_{2\times2}]^{-1}\phi(t)^TP_{t-1} \tag{13}$$

a parameter update

$$\hat{\theta}_t=\hat{\theta}_{t-1}+P(t)\phi(t)\varepsilon(t,\hat{\theta}_{t-1}) \tag{14}$$

and initialized at $t=1$ by $\theta_0=0$ and $P_0=\mu I$, $\mu\gg1$. Typically, one chooses μ to be a large number to allow for fast and aggressive initial parameter updates [17].

Unfortunately, the standard RLS formulation as given above suffers from two main drawbacks: (a) Choosing a large value of $\mu \gg 1$ to allow for fast initial parameter updates θ_t causes a large volatility in $\theta_t - \theta_{t-1}$ during the initial parameter updates and (b) for $\mu \gg 1$, $\lim_{t\to\infty} P_t = 0$, causing the parameter updates to converge to a stationary point $\lim_{t\to\infty}\theta_t = \theta^\star$. Item (a) is problematic, since the parameter θ_t is used directly in the controller perturbation $Q(q,\theta_t)$ and causes large volatility in the controller updates C_Q and the resulting control signal $u(t) = -C_Q y(t)$, possibly saturating or destabilizing the time varying control system.

To address drawback (a), the controller perturbation $Q(q,\tilde{\theta}_t)$ is updated with a parameter $\tilde{\theta}_t$ that is a *time-filtered version* of the estimated parameter $\hat{\theta}_t$ according to

$$\tilde{\theta}_t = (1-\delta)\hat{\theta}_t + \delta\tilde{\theta}_{t-1} \tag{15}$$

where $0 \le \delta < 1$. The closer δ is to 1, the more filtering and the slower the parameter $\tilde{\theta}_t$ is adjusted due to step-wise changes in $\hat{\theta}_t$.

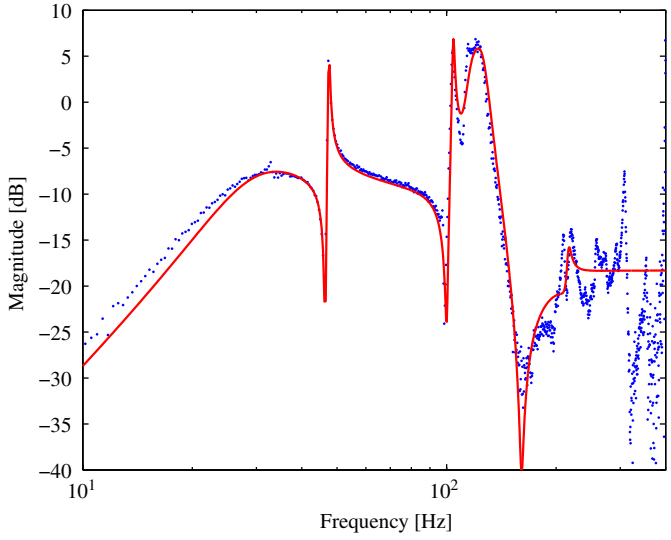

Fig. 1. Amplitude Bode response of the estimated frequency response (dotted line) and estimated 14th order model $\hat{G}$ (solid line).

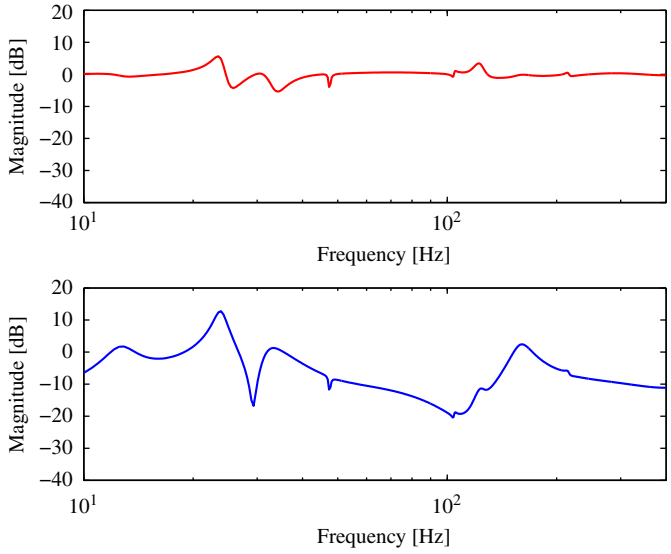

Fig. 2. Nominal performance evaluation of the initial controller C_i via the amplitude Bode response of the sensitivity $(1+\hat{G}C_i)^{-1}$ (top, solid/red line) and the input sensitivity $C_i(1+\hat{G}C_i)^{-1}$ (bottom, solid/blue line). (For interpretation of the references to color in this figure legend, the reader is referred to the web version of this article.)

It allows for smooth controller parameter updates, despite a large initialization of the parameter covariance matrix P_0.

To address drawback (b), a regularization is added to the time weighted covariance update P_t in (13) according to

$$P_t = P_{t-1} + \lambda_0 I - P_{t-1}\phi(t)[\phi(t)^T P_{t-1}\phi(t) + I_{2\times 2}]^{-1}\phi(t)^T P_{t-1} \tag{16}$$

where $\lambda_0 > 0$. The regularization has a close relation to Kalman filtering updates when parameters are time varying [17] and ensure $P_t > 0$, even as $t \to \infty$. This means that the parameter estimate θ_t will not converge to a stationary point, and is able to change at any time t in case there is a change in the spectrum $\Phi_v(\omega) = |H(e^{j\omega})|^2\nu$ of the noise disturbance $v(t) = He(t)$.

2.5. Dealing with model uncertainty

The Youla–Kucera parametrization as given in Definition 1 assumes no modelling error or uncertainty on the model dynamics $\hat{G}$ to ensure stability of the newly tuned or perturbed controller C_Q.

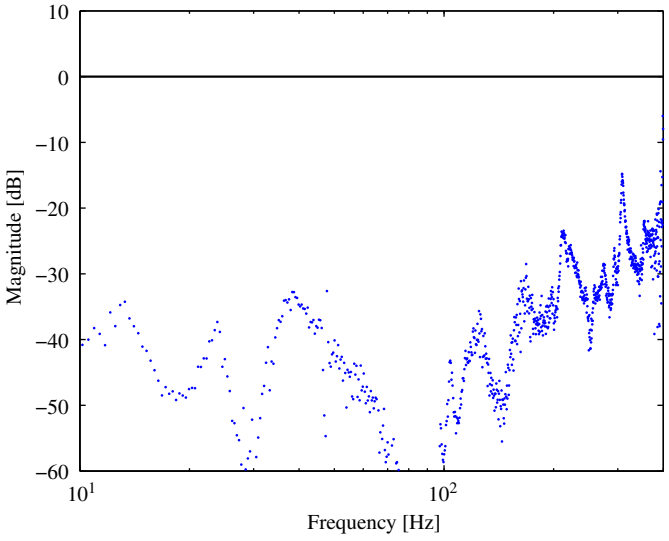

Fig. 3. Additive uncertainty robust stability test by evaluation of (22) over the frequency grid ω_k, $k = 0, 1, \ldots, N/2$ in (21).

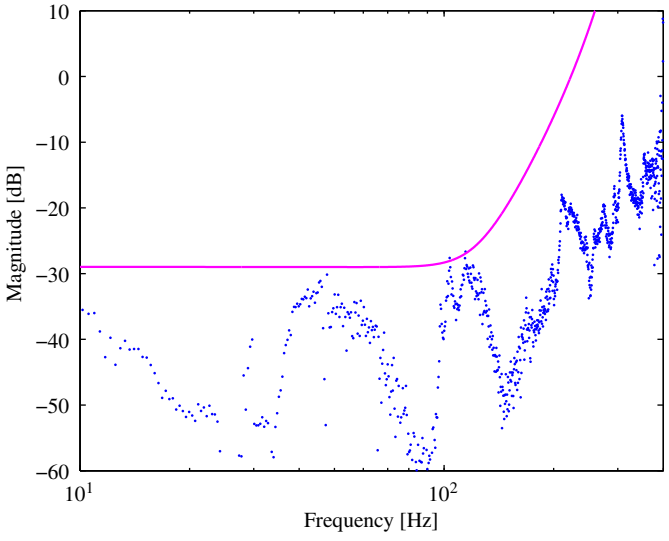

Fig. 4. Evaluation of the amplitude Bode response of the $\Delta(\omega_k)$ as given in (19) (dotted/blue line) and amplitude Bode response of the control input weighting filter W (solid/magenta line). (For interpretation of the references to color in this figure legend, the reader is referred to the web version of this article.)

As a result, the only requirement for stability robustness is the stability of the Youla–Kucera parameter Q. In case of discrepancy between a nominal model $\hat{G}$ and the actual plant dynamics G, an additional constraint on the actual "size" of Q will have to be imposed to guarantee stability robustness. Following the ideas of a double-Youla parametrization [19], uncertainty on the model dynamics $\hat{G}$ can also written in a coprime framework. This allows a clear computation of the upper bound on the size of the Youla–Kucera Q in the (weighted) REACT algorithm. The results are summarized as a corollary here [7].

Corollary 3. *Consider a nominal model $\hat{G}$ of a system G and an initial controller C_i with $T(C_i,\hat{G})\in\mathcal{RH}_\infty$ and $T(C_i,G)\in\mathcal{RH}_\infty$. Let $\mathcal{P}$ be the set of models given by*

$$\mathcal{P}=\{P|P=(N+D_i\Delta)(D-N_i\Delta)^{-1},\quad \text{where } \|V^{-1}\Delta\|_\infty\le 1\} \tag{17}$$

where (N,D) is a rcf of $\hat{G}$, (N_i,D_i) is a rcf of C_i and V over-bounds the model error $\Delta=D_i^{-1}(I+GC)^{-1}[G-\hat{G}]D$. A controller $C_Q=N_QD_Q^{-1}$ with

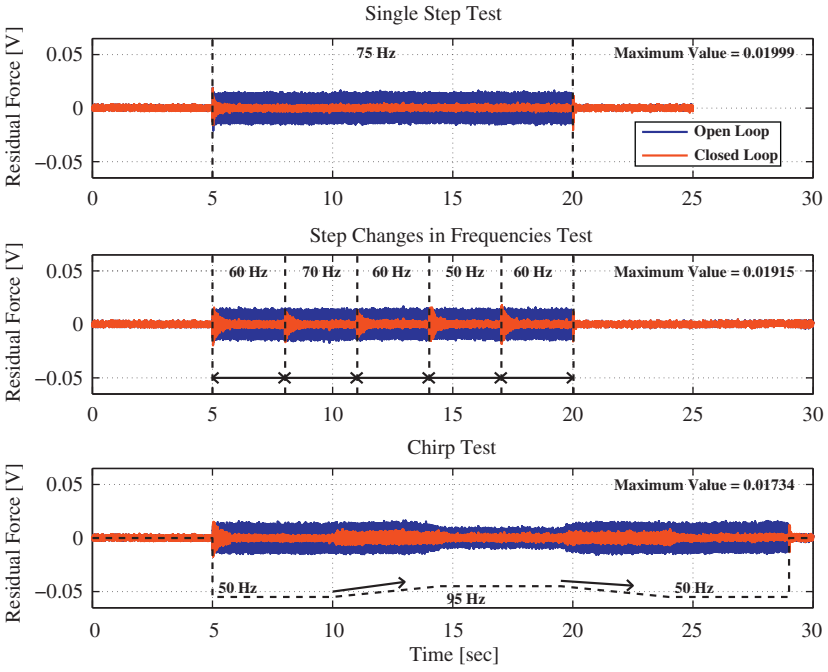

Fig. 5. Simulation results of open loop (blue) and closed-loop (red) output time sequences for a Level 1 SST (top), SCFT (middle) and CT (bottom). The frequency of the single harmonic disturbances and the maximum values of the output signal in closed-loop are indicated in the figure. (For interpretation of the references to color in this figure legend, the reader is referred to the web version of this article.)

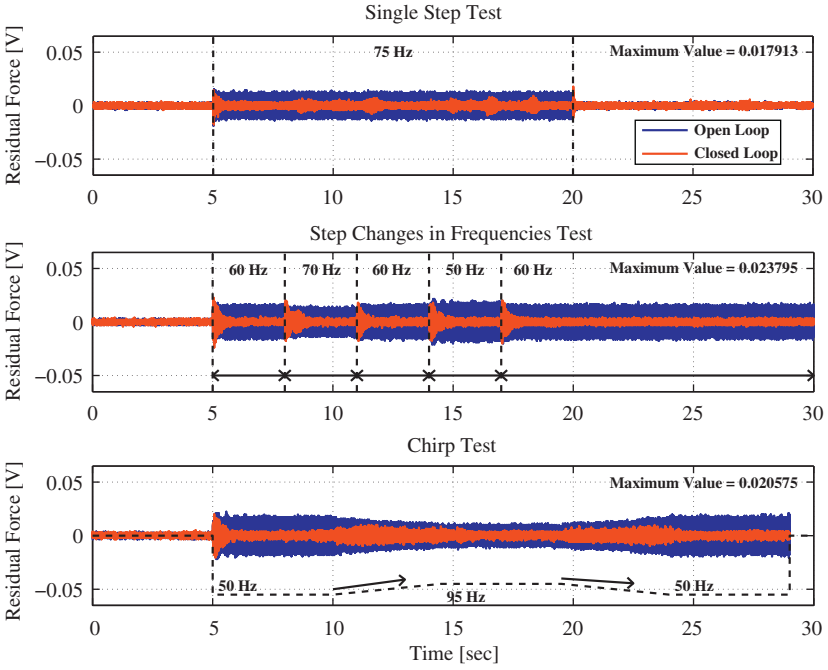

Fig. 6. Experimental results of open loop (blue) and closed-loop (red) output time sequences for a Level 1 SST (top), SCFT (middle) and CT (bottom). The frequency of the single harmonic disturbance and the maximum values of the output signal in closed-loop are indicated in the figure. (For interpretation of the references to color in this figure legend, the reader is referred to the web version of this article.)

a rcf

$$N_Q = N_i + DQ$$
$$D_Q = D_i - NQ, \tag{18}$$

satisfies $T(C_Q, P) \in \mathcal{RH}_\infty \forall P \in \mathcal{P}$ if and only if $Q \in \mathcal{RH}_\infty$ and $\|QV\|_\infty < 1$.

The proof of Corollary 3 follows the arguments of the small gain theorem [27,7] and indicates that $\|Q(\theta)V\|_\infty < 1$ for a constant θ is a necessary and sufficient to stabilize all plants P contained in the set $\mathcal{P}$ defined in (17). The result in Corollary 3 indicates that next to the stability requirement on Q mentioned in Definition 1, there is now also a 'size' constraint on Q measured by an $\mathcal{H}_\infty$-norm. If there is no uncertainty, $V=0$ and only the requirement on the stability of Q remains according to Definition 1. It should be noted that the robust stability result only holds for a constant parameter θ in $Q(\theta)$. Limiting the rate of change in the parameter $\tilde{\theta}_t$ for the actual update of $Q(\tilde{\theta}_t)$ via the filtering in (15) contributes to the stability robustness of the algorithm.

Although the uncertainty Δ on the model in (17) looks more complicated than a standard unstructured additive or multiplicative uncertainty, it is nothing else than a bound on the unstructured uncertainty on a *closed-loop transfer function*. In fact, if the system dynamics G was known, Δ can be computed exactly via

$$\Delta = D_i^{-1}(I + GC)^{-1}[G - \hat{G}]D \tag{19}$$

The so-called dual-Youla coprime factor uncertainty $P = (N + D_i\Delta)(D - N_i\Delta)^{-1}$, $\Delta \in \mathcal{RH}_\infty$ in (17) has a major advantage: it can describe unstructured uncertainty on both stable and unstable systems. As such, it even allows poles to perturb across the imaginary axis (or unit circle in discrete-time systems).

The presence of model uncertainty $\Delta(\omega)$ bounded by a frequency dependent function $V(\omega)$ would require a constrained minimization

$$\min_\theta \|\varepsilon(t,\theta)\|_2, \quad \text{subject to}$$
$$\left| \left(b_0 + \sum_{k=0}^{\bar{k}-1} b_{k+1} e^{-(k+1)j\omega} \right) V(e^{j\omega}) \right| < 1 \tag{20}$$

with $\varepsilon(t,\theta)$ given in (7). The quadratic minimization subject to an amplitude constraint in (20) can be written in a quadratically constraint quadratic programming (QCQP) problem, when evaluating the amplitude constraint over a dense frequency grid. The QCQP problem may be solved via Semi Definite Programming (SDP) and specialized software for second order cone programming [4] can be used to solve the QCQP off-line.

Stability during adaptation can be enforced explicitly if the QCQP can be solved in real-time. Instead, we use a RLS solution that has been extended with a weighting filter $\gamma W(q)$ on the control signal u. Choosing $\gamma|W(qe^{j\omega})|$ to be large in a particular frequency region will implicitly control the size of $|Q(e^{j\omega})|$ to satisfy

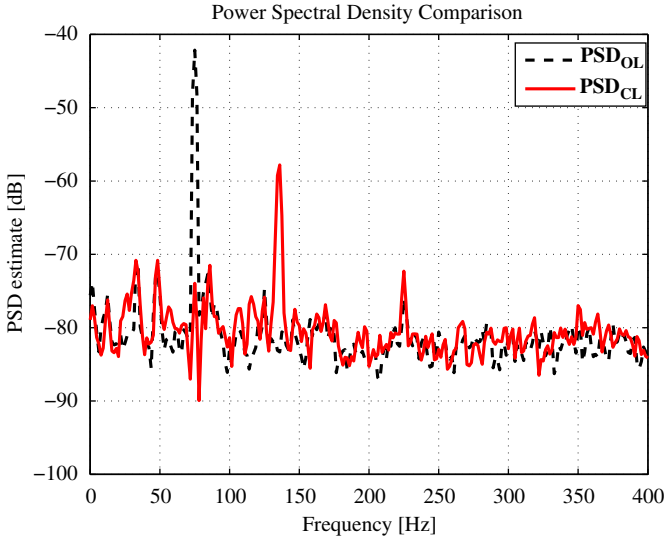

Fig. 7. Experimental results of the open loop (dashed black line) and closed-loop (red line) Power Spectral Density (PSD) estimates of the converged output signal in case of a Level 1 SST. (For interpretation of the references to color in this figure legend, the reader is referred to the web version of this article.)

Table 1
Performance and transient results for a Level 1 SST with $\bar{k} = 29$ in (8).

Freq. (Hz)	G_A (dB)	D_A (dB)	M_A (dB@Hz)	T_N (10^{-3} V^2)	R_N (10^{-3} V^2)	T_M (mV)	α (–)
Simulation							
50	33.64	40.99	4.29@67.19	22.09	3.99	19.26	1.0409
55	33.19	37.68	4.45@71.88	21.82	4.23	21.64	1.0389
60	32.86	35.78	4.43@46.88	20.62	4.39	21.17	1.0287
65	33.06	34.71	4.62@112.50	17.23	4.36	18.30	1.0212
70	33.30	34.07	4.47@31.25	12.39	4.30	19.04	1.0173
75	33.78	33.61	4.36@31.25	10.88	4.15	19.99	1.019
80	34.03	33.13	4.73@104.70	14.39	3.99	21.45	1.0355
85	33.80	32.53	4.56@109.40	21.73	3.96	23.73	1.0514
90	31.65	30.89	5.27@112.50	25.13	4.17	27.46	1.0306
95	23.10	25.23	6.35@129.70	19.49	4.97	32.01	1.0137
Experiment							
50	36.53	40.31	12.97@131.30	40.45	5.36	21.33	0.9092
55	34.69	36.70	8.65@132.80	30.68	4.86	22.59	0.91322
60	34.26	35.06	10.72@132.80	31.58	4.53	22.58	1.1945
65	29.69	33.57	19.96@134.40	22.36	6.32	19.10	1.0436
70	28.79	32.73	13.72@134.40	19.86	6.00	20.37	1.0849
75	24.50	31.79	25.51@135.90	11.17	8.94	17.91	0.89367
80	24.92	31.24	24.72@135.90	9.94	8.05	20.06	0.80793
85	28.83	30.21	14.45@137.50	8.75	4.89	18.86	0.97769
90	22.19	28.03	23.63@135.90	12.83	9.39	22.53	0.58935
95	23.05	23.60	10.66@103.10	17.61	6.65	22.81	1.0459

Table 2
Performance and transient results for a Level 1 SCFT experiments with $\bar{k} = 29$ in (8).

S#	Freq. (Hz)	T_N (10^{-3} V^2)	T_M (mV)
Simulation			
S1	60→70	13.70	17.58
	70→60	13.23	14.40
	60→50	21.65	16.11
	50→60	21.18	19.15
S2	75→85	16.19	15.12
	85→75	13.11	15.01
	75→65	14.06	13.89
	65→75	15.62	14.84
S3	85→95	12.20	17.87
	95→85	19.34	24.34
	85→75	13.96	15.92
	75→85	12.71	14.68
Experiment			
S1	60→70	27.95	20.32
	70→60	22.62	17.87
	60→50	31.29	17.87
	50→60	22.56	23.80
S2	75→85	18.38	15.71
	85→75	23.38	16.16
	75→65	22.68	19.83
	65→75	32.33	16.93
S3	85→95	15.02	16.90
	95→85	24.86	19.86
	85→75	24.35	13.74
	75→85	18.29	17.41

$\|Q(e^{j\omega},\theta)V(e^{j\omega})\|_\infty < 1\ \forall\omega$. For the benchmark problem it will be shown that the weighting function W will be chosen according to the shape of the model uncertainty Δ given in (19).

3. Application to vibration benchmark

3.1. Summary of benchmark

The mechanical test bed of the benchmark on adaptive regulation [13,14] is used to verify the proposed weighted REACT algorithm for adaptive regulation of disturbances. Disturbances enter the mechanical system via a Primary Path (PP) actuator, while feedback control can be done via a Secondary Path (SP) actuator. Only an approximate model of the SP actuator is used, the dynamics of the PP actuator is assumed to be unknown during the weighted REACT algorithm for adaptive regulation. The benchmark problem requires adaptive regulation of multiple unknown and time-varying harmonic disturbances in the range between 50 and 100 Hz at different levels of complexity.

The *levels* of complexity in the benchmark are distinguished by the *number of harmonic disturbances* that may be present at any given time, varying from a single frequency sinusoidal disturbance (Level 1) to sinusoidal disturbances with three distinct frequencies (Level 3). For each level of complexity we also consider different time-varying effects of the disturbance. Simple Step Test (SST) experiments are used to study the performance of the adaptive regulation in case the disturbances is applied in a step-wise fashion. In our Step Changes in Frequencies Test (SCFT) experiments, the frequency contents of the harmonic disturbances varies multiple times in a step-wise fashion. Finally, Chirp Test (CT) experiments are used to inspect the performance of the weighted REACT in case the frequency contents of the (multiple) harmonic disturbances change linearly up and down during the experiment. More details on the different levels of complexity and performance measures for the adaptive regulation can be found in the description of the vibration benchmark at [13].

3.2. Plant dynamics and initial controller design

As indicated before, only a model $\hat{G}$ of the SP actuator is used in the weighted REACT algorithm, e.g. the PP actuator is assumed to be unknown and its frequency response is part of the spectral contents of the unknown disturbance dynamics. For estimation of the model $\hat{G}$, open loop measurements $\{u,y\}$ of the SP actuator sampled at 800 Hz are used. Experiment design was outside the scope of the benchmark problem and an open-loop input $u(t)$ consisting of four periodically applied Pseudo Binary Sequences of $N=2046$ data points was applied to the SP actuator. The periodic

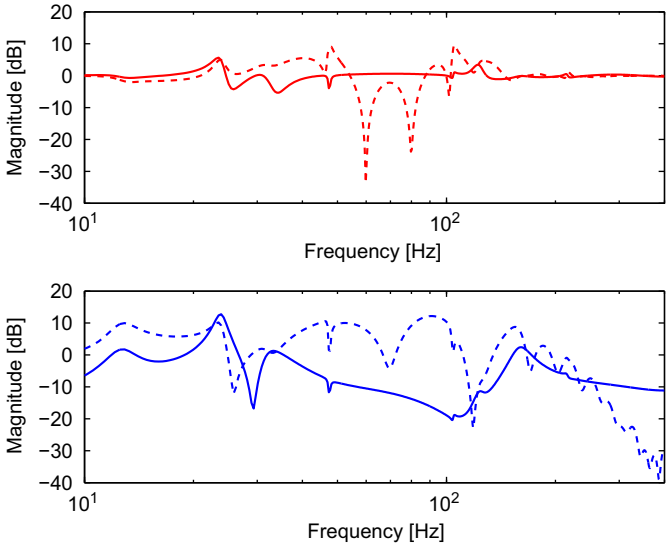

Fig. 9. Amplitude Bode response of the sensitivity $(1+\hat{G}C(Q))^{-1}$ (top, dashed/red line) and input sensitivity $C(Q)(1+\hat{G}C(Q))^{-1}$ (bottom, dashed/blue line) due to adaptive regulation at $t=15$sec for the Level 2 SST simulation. The amplitude Bode responses are compared with the initial sensitivity $(1+\hat{G}C_i)^{-1}$ and input sensitivity $C_i(1+\hat{G}C_i)^{-1}$ (solid lines) given earlier in Fig. 2. (For interpretation of the references to color in this figure legend, the reader is referred to the web version of this article.)

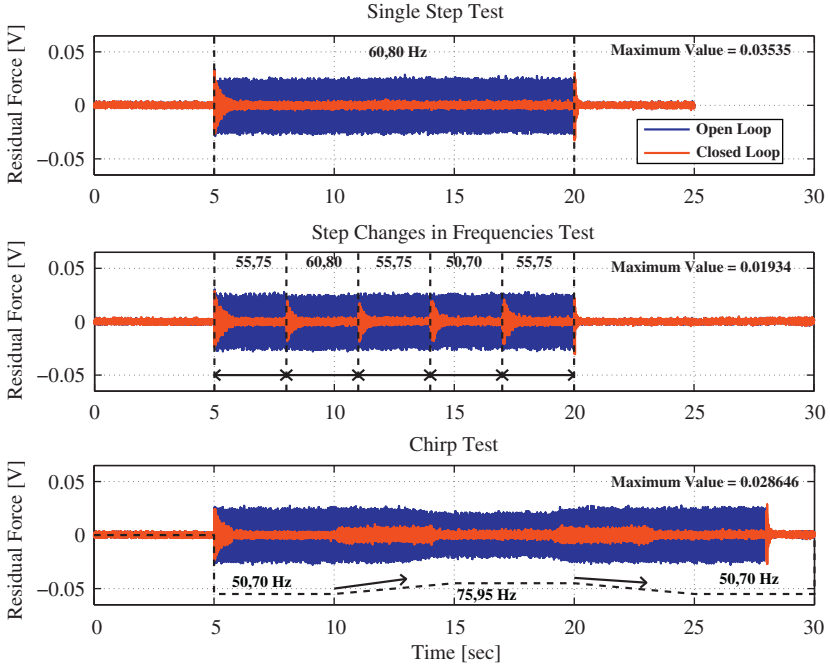

Fig. 8. Simulation results of open loop (blue) and closed-loop (red) output time sequences for a Level 2 SST (top), SCFT (middle) and CT (bottom). The two frequencies of the harmonic disturbances and the maximum values of the output signal in closed-loop are indicated in the figure. (For interpretation of the references to color in this figure legend, the reader is referred to the web version of this article.)

input signal allows direct Discrete-Time Fourier Transform (DTFT) $U(\omega_k), k=0,1,\ldots,N/2$, over a single period of $N=2046$ data points without initial- and end-condition effects. Computing the DTFT $Y_l(\omega_k)$ of the output $y(t)$ over the four different periods $l=1,\ldots,4$ allows the computation of an averaged Empirical Transfer Function Estimate (ETFE)

$$G(\omega_k)=\frac{1}{4}\frac{\sum_{l=1}^{4}Y_l(\omega_k)}{U(\omega_k)} \tag{21}$$

as an estimate of the frequency response $G(\omega_k)\in\mathbb{C}$ of the SP actuator. Knowing that disturbances will be in the range from 50 to 100 Hz, an approximate model $\hat{G}$ of the SP actuator is created based on standard frequency domain curve fitting. Choosing a frequency dependent weighting function $F(\omega_k)$ that emphasizes 50–100 Hz frequency range, a discrete-time model $\hat{G}=G(q,\hat{\theta})$ is estimated by minimizing

$$\hat{\theta}=\arg\min_{\theta}\sum_{k=0}^{N/2}|(G(\omega_k)-G(e^{j\omega_k},\theta))F(\omega_k)|^2$$

using an iterative least squares optimization routine [26]. A trade-off is made between model order to facilitate real-time implementation and the resulting model error in the frequency domain. In order to capture some of the main resonance modes in the SP actuator, a 14th order model $\hat{G}$ is estimated via the curve fitting and the results are summarized in Fig. 1. It can be observed that the SP actuator has several resonance modes in the range 0–400 Hz (Nyquist frequency). Approximations and thus modelling errors are present at most of the resonance modes and the effect of a poorly damped non-minimum phase zero around 98 Hz has been captured in the model.

The proposed adaptive regulation algorithm can include the knowledge of a possible initial controller C_i. Although C_i can be chosen to be zero as the plant G and the model $\hat{G}$ are stable, the model $\hat{G}$ is used to design an initial stable discrete-time controller C_i via a standard $\mathcal{H}_2$ control design [27]. Without knowledge (yet) of the disturbance $v(t)$ that will act on the feedback system, the initial controller C_i is designed to minimize (4) in the presence of a white noise disturbance signal $v(t)$. It is clear that the initial controller C_i will be far from optimal for the actual disturbances seen in the benchmark problem. A final step in the design of C_i is reducing the controller order. Via truncation of a balanced state space realization, while monitoring stability of the closed-loop system $T(C_i,\hat{G})$ and the shape of the sensitivity function $(1+\hat{G}C_i)^{-1}$, the order of the initial controller C_i could be reduced to order 11.

For a final check of the initial controller C_i, it should be verified that C_i also stabilizes the actual plant G (SP actuator), as $T(C_i,G)\in\mathcal{RH}_\infty$ is required for the Youla–Kucera parametrization. Without any knowledge of a stabilizing controller for the actual

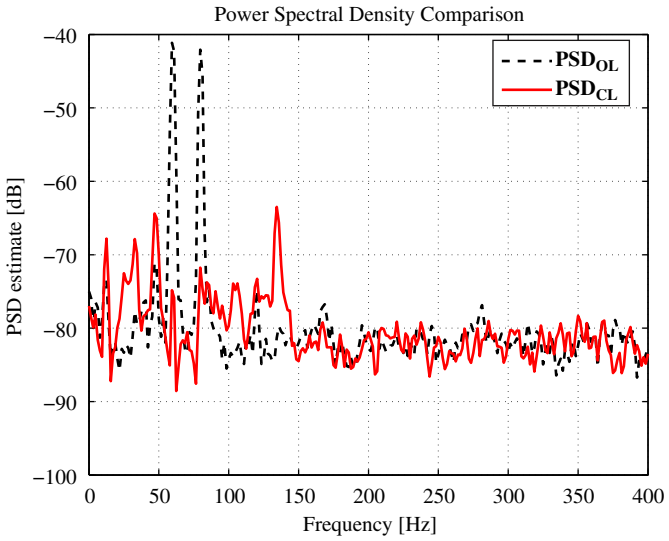

Fig. 11. Experimental results of the open loop (dashed black line) and closed-loop (red line) Power Spectral Density (PSD) estimates of the converged output signal in case of a Level 2 SST. (For interpretation of the references to color in this figure legend, the reader is referred to the web version of this article.)

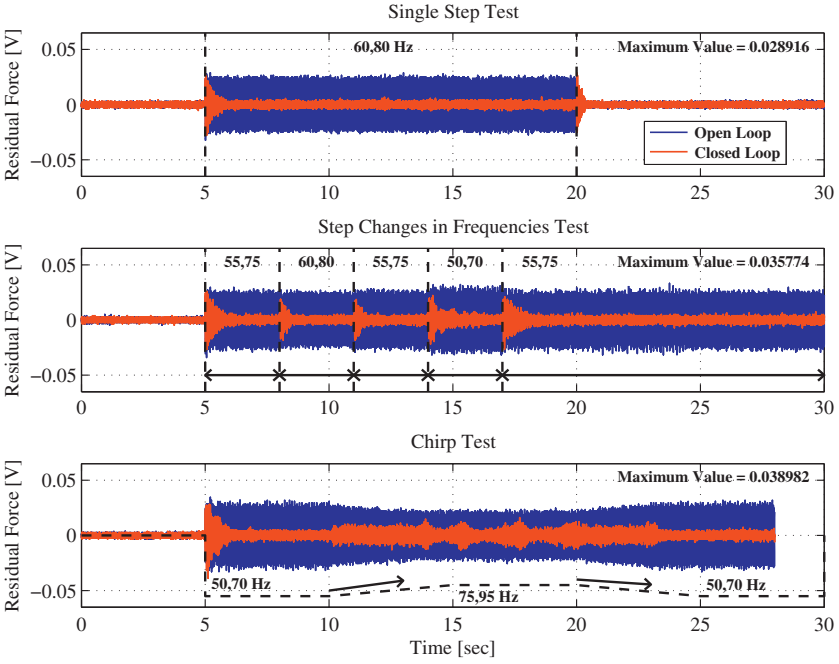

Fig. 10. Experimental results of open loop (blue) and closed-loop (red) output time sequences for a Level 2 SST (top), SCFT (middle) and CT (bottom). The two frequencies of the harmonic disturbances and the maximum values of the output signal in closed-loop are indicated in the figure. (For interpretation of the references to color in this figure legend, the reader is referred to the web version of this article.)

plant G, the double-Youla parametrization in Corollary 3 cannot be applied and one has to resort to an open-loop based robust stability test. Using the small gain theorem [27] with an additive model uncertainty description $\Delta_a(\omega)=G(\omega)-\hat{G}(\omega)$ and the fact that $(1+\hat{G}C_i)^{-1}\in RH$, a sufficient test for stability of $T(C_i,G)$ is given by the Frequency Domain Inequality (FDI)

$$\left|\Delta_a(\omega)\frac{C_i(\omega)}{1+\hat{G}(\omega)C_i(\omega)}\right|<1\ \forall\omega \tag{22}$$

For the proper evaluation of the FDI, $\Delta_a(\omega)$ could be overbounded by a stable and stably invertible discrete-time filter and compute the value of the left hand side of (22) via an $\mathcal{H}_\infty$ norm. A good (qualitative) indication of the stability robustness properties of C_i applied on the actual plant G can also be obtained by computing the left hand side of (22) over the dense frequency grid $\omega_k, k=0,1,\ldots,N/2$ for which we have frequency domain measurements of $G(\omega_k)$ in (21).

The results on the nominal performance and robust stability of the initial controller C_i are summarized in Figs. 2 and 3. It can be observed from the Amplitude Bode response of the sensitivity function $(1+\hat{G}C_i)^{-1}$ in Fig. 2 that the initial controller gives little initial disturbance rejection in the frequency range between 50 and 100 Hz and that adaptation must be used to improve (harmonic) disturbance rejection. The robust stability test in Fig. 3 indicates that the initial controller C_i does stabilize the plant, allowing the application of the double-Youla parametrization in Corollary 3.

3.3. Design choices in weighted REACT

The filtered signals u_f and y_f in (10) are obtained by choosing the rcf (N,D) of $\hat{G}$ and the rcf (N_i,D_i) of C_i as normalized coprime factorizations [27]. The choice of normalized coprime factorizations has two main advantages. Firstly, the dynamics of the filters used in the operation in (10) is determined by the closed-loop poles of the feedback connection $T(C_i,\hat{G})$ due to the presence of Λ_i and the poles of the coprime factors (N,D) and (N_i,D_i). Choosing the coprime factors normalized makes sure the filters for the two signals u_f and y_f are scaled similarly. Secondly, the additional poles in the coprime factors D_i and D shape the dual-Youla coprime factor uncertainty Δ in (19) to account for controller and plant dynamics.

To facilitate real-time implementation, the controller perturbation $Q(\theta)$ is parameterized as (8) with $\bar{k}=29$. Choosing $\bar{k}$ larger allows more freedom in adapting the controller C_Q, especially for multiple harmonic disturbances at higher level of complexity of the benchmark. For the real-time implementation sampled at 800 Hz, the size of $\bar{k}$ was limited to $\bar{k}=29$ by the available computational power to implement the recursive estimation of the parameter $\hat{\theta}_t$ via the three computational steps outlines in (12), (16) and (14).

With the frequency domain measurements $G(\omega_k)$ in (21), knowledge of the initial controller C_i with its rcf (N_i,D_i) and the model $\hat{G}$ with its rcf (N,D), the dual-Youla coprime factor uncertainty $\Delta(\omega_k)$ in (19) can be evaluated over the frequency grid $\omega_k,\ k=0,1,\ldots,N/2$. It will provide information on the allowable size of the controller perturbation $Q(e^{j\omega_k},\theta)$ parametrized by the FIR filter in (8) due to a size constraint

$$\min_\theta \|\varepsilon(t,\theta)\|_2,\quad \text{subject to}$$
$$\left|\left(b_0+\sum_{k=0}^{\bar{k}-1}b_{k+1}e^{-(k+1)j\omega_k}\right)\Delta(e^{j\omega_k})\right|<1$$

similar to (20).

To ensure that the controller C_Q is robust against unmodelled dynamics above 150 Hz in $\hat{G}$, the size of $Q(e^{j\omega_k},\theta)$ is bounded implicity via the weighting function W used for measuring the norm of the weighted control signal u_w in (4). The *monic* filter W

Table 4
Performance and transient results for Level 2 SCFT experiments with $\bar{k}=29$ in (8).

S#	Freq. (Hz)	T_N (10^{-3} V^2)	T_M (mV)
Simulation			
S1	55;75→60;80	13.76	18.94
	60;80→55;75	14.19	17.24
	55;75→50;70	19.14	17.72
	50;70→55;75	17.62	19.34
S2	70;90→75;95	16.23	20.59
	75;95→70;90	20.06	24.38
	70;90→65;85	15.16	19.23
	65;85→70;90	14.22	16.67
Experiment			
S1	55;75→60;80	19.10	18.62
	60;80→55;75	21.55	18.62
	55;75→50;70	42.09	22.29
	50;70→55;75	47.26	26.73
S2	70;90→75;95	25.76	13.70
	75;95→70;90	34.91	20.62
	70;90→65;85	23.62	18.60
	65;85→70;90	33.15	18.60

Table 3
Performance and transient results for Level 2 SST with $\bar{k}=29$ in (8).

Freq. (Hz)	G_A (dB)	D_A (dB)	M_A (dB@Hz)	T_N (10^{-3} V^2)	R_N (10^{-3} V^2)	T_M (mV)	α (–)
Simulation							
50;70	38.51	39.15;33.13	6.11@31.25	37.54	4.59	26.39	1.0006
55;75	38.43	36.78;32.70	6.15@129.70	37.77	4.70	31.33	1.0012
60;80	38.33	34.53;32.14	7.17@48.44	40.13	4.73	35.35	1.0298
65;85	37.73	33.55;31.29	8.72@104.70	60.46	5.02	38.14	1.0184
70;90	37.08	33.48;30.12	7.28@109.40	45.75	4.96	40.17	1.0036
75;95	33.20	32.68;23.92	8.70@103.10	38.35	5.92	44.29	0.99795
Experiment							
50;70	36.96	36.41;31.44	11.05@90.63	69.99	8.04	36.03	1.0671
55;75	34.79	35.46;30.59	16.29@132.80	47.19	7.97	30.14	1.0659
60;80	33.73	33.69;29.69	17.83@134.40	41.83	8.00	28.92	0.85115
65;85	28.29	29.04;26.64	14.61@132.80	61.29	13.20	31.17	0.71995
70;90	27.13	30.13;24.30	21.29@103.10	42.02	13.52	34.83	0.80419
75;95	23.09	29.71;19.80	24.59@132.80	51.50	19.33	36.06	0.63188

in (4) is chosen as

$$W(q) = \frac{q^4 - 1.57q^3 + 1.276q^2 - 0.4844q + 0.0762}{q^4 + 2.8q^3 + 2.94q^2 + 1.372q + 0.2401} \quad (23)$$

representing a 4th order high-pass filter with a cut-off frequency at 150 Hz, a DC-gain of −30 dB and a gain of 50 dB at the Nyquist frequency of 400 Hz. An amplitude Bode plot of $\Delta(\omega_k)$ in (19) evaluated over the available frequency grid and the chosen 4th filter $W(e^{j\omega_k})$ in (23) are summarized in Fig. 4. To further limit the control signal during adaptation, the value of γ is set to $\gamma = 1.4$. The choice of $\gamma = 1.4$ is confirmed with simulation results and ensured that the control signal $u(t)$ remains within the bounds of $\pm 0.5\ V$ during adaptation. These choices for W and γ will be kept the same during all adaptive regulation experiments of C_Q.

It can be seen from Fig. 4 that $\Delta(\omega_k)$ is smaller in the range 10–100 Hz and W is chosen to be small in that same frequency range. The high-pass character of W will avoid a large $Q(e^{j\omega_k}, \theta)$ for higher frequencies during controller adaptation. Clearly, choosing a weighting W and using a 2-norm minimization in (4) will not guarantee $\|Q(\theta)\Delta\|_\infty < 1$, but the weighting W does give a handle on the size of the controller perturbation $Q(\theta)$ during adaptive regulation.

To avoid effects of the initial parameter conditions during adaptation, the controller $C_Q(\tilde{\theta}_t)$ is updated with the filtered parameter $\tilde{\theta}_t$ in (15). For the recursive adaptation with the weighted REACT, a fixed initialization is chosen with $\hat{\theta}_t = 0$ and $P_0 = \mu I$, $\mu = 10^4$ and $\delta = 0.995$ in (15) and $\lambda_0 = 2$ in (16) at 800 Hz sampling. The choice of $\delta = 0.995$ for the filtering of the parameter estimates will smoothen the volatility when the adaptive regulation controller is initialized and/or adjusted to reduce periodic disturbances with sudden jumps in the frequency content. The value of $\lambda_0 = 2$ allows for reasonable fast perturbations of the parameter update $\hat{\theta}_t$ in case of sudden jumps in the disturbance spectra, while allowing small enough perturbations of the parameter update $\hat{\theta}_t$ during convergence. The initialization at $\theta_0 = 0$ allows the controller C_Q to start at the initial controller C_i, while a large value of $\mu = 10^4$ allows fast parameter updates at the start of the adaptation.

3.4. Simulation and real-time results for Level 1 experiments

For the initial evaluation of the weighted REACT algorithm, a harmonic disturbance with only one frequency (Level 1) in the range 50–95 Hz is applied at an unknown time. During the absence and presence of the harmonic disturbance, the controller C_Q is required to regulate itself to minimize the criteria in (4). The typical performance and transient effects of the weighted REACT algorithm during a simulation are summarized in Fig. 5, where

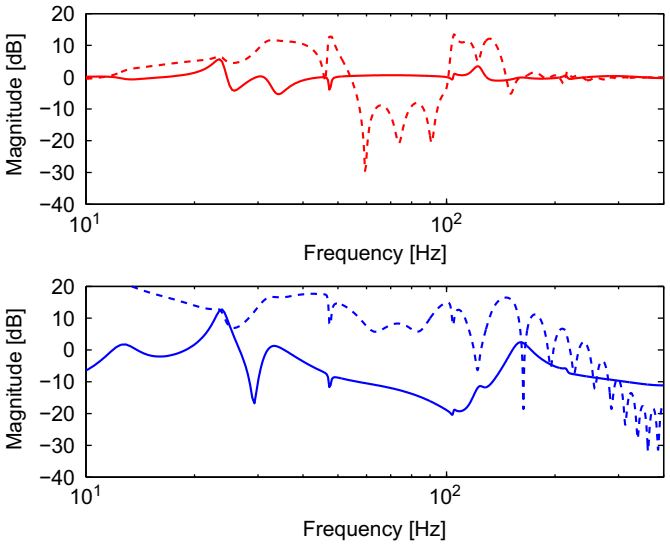

Fig. 13. Amplitude Bode response of the sensitivity $(1 + \hat{G}C(Q))^{-1}$ (top, dashed/red line) and input sensitivity $C(Q)(1 + \hat{G}C(Q))^{-1}$ (bottom, dashed/blue line) due to adaptive regulation at $t = 15$ s for the Level 3 SST simulation. The amplitude Bode responses are compared with the initial sensitivity $(1 + \hat{G}C_i)^{-1}$ and input sensitivity $C_i(1 + \hat{G}C_i)^{-1}$ (solid lines) given earlier in Fig. 2. (For interpretation of the references to color in this figure legend, the reader is referred to the web version of this article.)

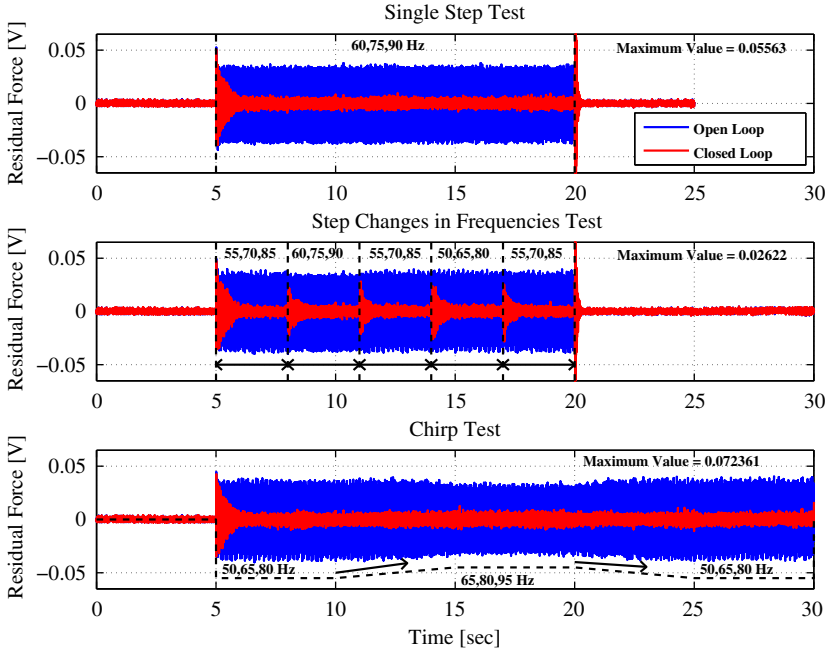

Fig. 12. Simulation results of open loop (blue) and closed-loop (red) output time sequences for a Level 3 SST (top), SCFT (middle) and CT (bottom). The three frequencies of the harmonic disturbances and the maximum values of the output signal in closed-loop are indicated in the figure. (For interpretation of the references to color in this figure legend, the reader is referred to the web version of this article.)

both a Simple Step Test (SST), Step Changes in Frequencies Test (STFT) and a Chirp Test (CT) are used as harmonic disturbances. The simulation results are based on models for the Primary Path (PP) and Secondary Path (SP) actuators provided by the benchmark [13] and indicate excellent disturbance reduction with transient durations that are typically less than 0.5 s.

Real-time implementation of the weighted REACT algorithm on the vibration benchmark shows good agreement between simulation and experimental results, as indicated in Fig. 6. This is also confirmed by the Power Spectral Density (PSD) estimate of the controlled output signal in the SST experiment depicted in Fig. 7 for a Level 1 disturbance. The spectral analysis that reveals excellent disturbance rejection of the 75 Hz harmonics, but also shows an amplification in neighboring frequencies. It also shows that the choice of the high pass filter $W(q)$ in (23) limits the control energy with no observable amplification of the PSD above 150 Hz. As noted before, additional modifications of the filter $W(q)$ or extending the parametrization of $Q(q,\theta)$ with a fixed stable denominator will allow for additional limitations of the control to a specific frequency range.

Similar results are also obtained for other harmonic disturbances with only one frequency (Level 1) in the range 50–95 Hz. A summary of the performance and transient effects for the different Level 1 disturbances is summarized in Tables 1 and 2 by the following parameters.

Definition 2. Let y_{ol} be the open-loop (no control) output signal and y_{cl} be the closed-loop (with adaptive control) output signal. Furthermore, let $L_i=4001$ indicate the first sample and $L_e=16\,000$ indicate the last sample for which the disturbance was present at the SST. Using 3 s of data at 800 Hz sampling, the global performance is measured via the global attenuation

$$G_A = 20\log^{10}\frac{\sum_{t=L_e-2400}^{L_e} y_{ol}(t)^2}{\sum_{t=L_e-2400}^{L_e} y_{cl}(t)^2}$$

The specific Disturbance Attenuation D_A is defined by the reduction of the Power Spectral Density (PSD) estimate at the frequencies of the disturbance (see for example Fig. 7 at 75 Hz). The parameter M_A is defined as the maximum change in amplification of any other frequencies in the PSD. The size of the residual is measured by the residual norm $R_N=\sum_{t=L_e-2400}^{L_e} y_{cl}(t)^2$. Transient effects are characterized by inspecting the transient norm $T_N=\sum_{t=L_i}^{L_i+2400} y_{cl}(t)^2$ and the maximum value $T_M=\max_t |y_c l(t)|$ during transient. Finally, the transient ratio α is defined as

$$\alpha = \frac{\sum_{t=5601}^{8001} y_{cl}(t)^2}{\sum_{t=13\,601}^{16\,001} y_{cl}(t)^2}$$

measuring the ratio of norm of the residuals respectively between 7 and 10 s, and between 17 and 20 s at 800 Hz sampling.

The results in the tables indicate that for a Level 1 disturbance on average a 30 dB reduction of the disturbance is obtained, except

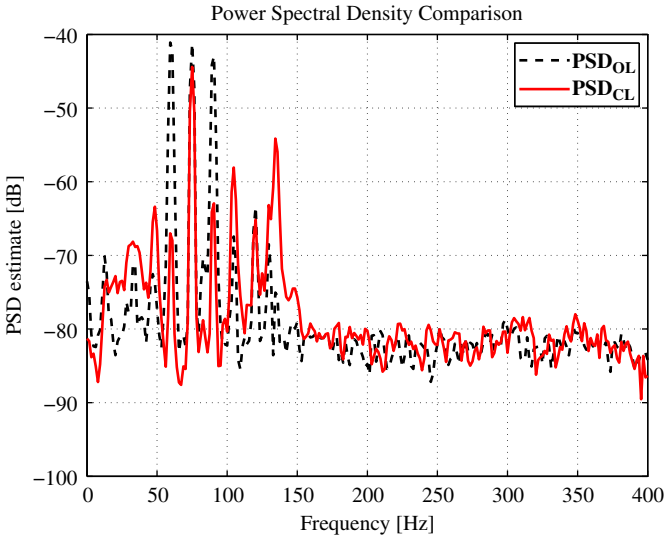

Fig. 15. Experimental results of the open loop (dashed black line) and closed-loop (red line) Power Spectral Density (PSD) estimates of the converged output signal in case of a Level 3 SST. (For interpretation of the references to color in this figure legend, the reader is referred to the web version of this article.)

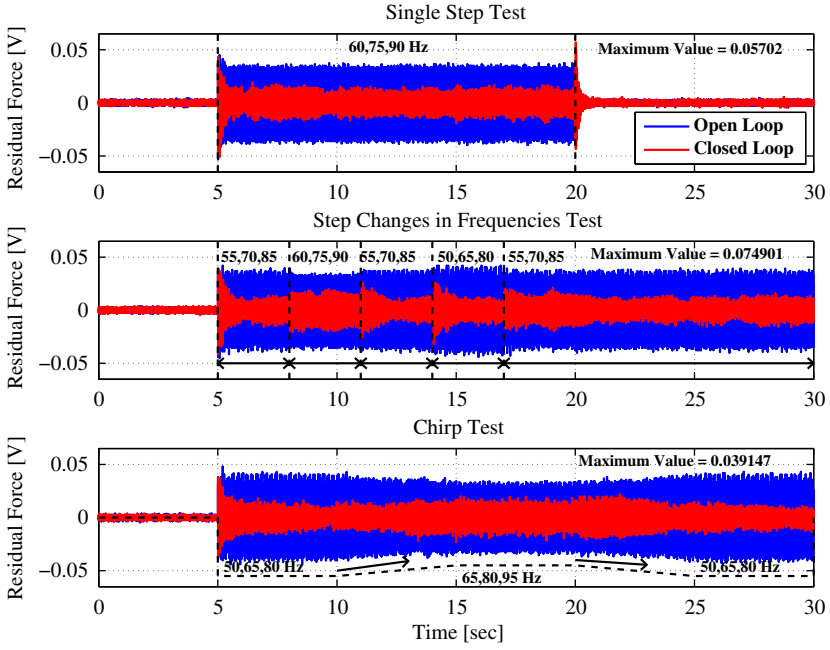

Fig. 14. Experimental results of open loop (blue) and closed-loop (red) output time sequences for a Level 3 SST (top), SCFT (middle) and CT (bottom). The three frequencies of the harmonic disturbances and the maximum values of the output signal in closed-loop are indicated in the figure. (For interpretation of the references to color in this figure legend, the reader is referred to the web version of this article.)

for the 95 Hz harmonic disturbance that is close to the undamped zero at 98 Hz in the SP actuator. The results in the tables indicate that the adaptive regulation with the weighted REACT can handle all possible combinations of a (single) harmonic disturbance in the experiments with a good converge as indicated by $\alpha < 1.2$ for all simulation and experiments. A value for α smaller than 1.2 indicates that specifications for transient duration are satisfied due to convergence within 2 s. A 30 dB reduction of the single periodic disturbance is obtained on average, while limiting amplification to less than 6.35 dB over the whole frequency range in simulation. During the experiments slightly smaller disturbance rejection and larger amplifications around 130 Hz were observed, most likely caused by the larger model uncertainty at this frequency, while not limiting the control energy with the control weighting function W at this frequency.

3.5. Simulation and real-time results for Level 2 experiments

To illustrate the effectiveness of the weighted REACT algorithm for two simultaneous harmonic disturbances, a typical simulation result for a Level 2 frequency disturbance is depicted in Fig. 8.

The adaptive regulation results with the weighted REACT for other Level 2 disturbance in the frequency range of 50–95 Hz look very similar to Fig. 8 with an excellent suppression of the sinusoidal disturbance down to the noise level of the experiment. The adaptive regulation of the harmonic disturbance can also be demonstrated by the computation of the (input) sensitivity functions $(1+\hat{G}C(Q))^{-1}$ and $C(Q)(1+\hat{G}C(Q))^{-1}$ and are given in Fig. 9. Comparing with the initial sensitivity function $(1+\hat{G}C_i)^{-1}$ and input sensitivity function $C_i(1+\hat{G}C_i)^{-1}$ given earlier in Fig. 2, the adaptive regulation with $Q=Q(\hat{\theta}_t)$ at $t=15$ s for the SST simulation has automatically created two notches in the frequency response of the sensitivity function $(1+\hat{G}C(Q))^{-1}$ to reduce the harmonic disturbances. The high-pass frequency weighting $\gamma W(q)$ on the control signal ensures that the input sensitivity function $C(Q)(1+\hat{G}C(Q))^{-1}$ decreases at higher frequencies.

Typical real-time implementation results of the weighted REACT algorithm on the vibration benchmark are summarized in Fig. 10. Disturbance rejection can be confirmed by the spectral analysis of the controlled output signal in the SST experiment depicted in Fig. 11 for a Level 2 disturbance. The spectral analysis that reveals excellent disturbance rejection of the two harmonics, but also shows an amplification in neighboring frequencies and no observable amplification of the PSD above 150 Hz due to the chosen input weighting filter $W(q)$. A summary of the performance and transient effects for the different Level 2 disturbances is summarized in Tables 3 and 4, indicating again on average 30 dB disturbance rejection, expect for a 95 Hz harmonic contribution. Similar smaller disturbance rejection and larger amplifications around 130 Hz were observed during the experiments.

3.6. Simulation and real-time results for Level 3 experiments

To complete the benchmark analysis, the simulation results for a Level 3 with three harmonic disturbances are depicted in Fig. 12.

The excellent suppression of the sinusoidal disturbance down to the noise level can again be demonstrated by the computation of the (input) sensitivity functions $(1+\hat{G}C(Q))^{-1}$ and $C(Q)(1+\hat{G}C(Q))^{-1}$ and given in Fig. 13. Comparing with the initial sensitivity function $(1+\hat{G}C_i)^{-1}$ given in Fig. 2, the adaptive regulation has now created three notches in the frequency response of the sensitivity function $(1+\hat{G}C(Q))^{-1}$ to reduce the harmonic disturbance at $t=15$ for the SST simulation. Again the high-pass frequency weighting $\gamma W(q)$ on the control signal ensures the input sensitivity function $C(Q)(1+\hat{G}C(Q))^{-1}$ decreases at higher frequencies.

The real-time implementation results of the weighted REACT algorithm for a Level 3 disturbance are summarized in Fig. 14. Disturbance rejection can be confirmed by the spectral analysis of the controlled output signal in the SCFT experiments depicted in Fig. 15 for a Level 3 disturbance. The spectral analysis of the controlled output signal in the SST depicted in Fig. 15 shows partial disturbance rejection of the three harmonic disturbances, with a similar amplification in neighboring frequencies. The partial

Table 6
Performance and transient results for Level 3 SCFT experiments with $\overline{k}=29$ in (8).

S#	Freq. (Hz)	T_N (10^{-3} V^2)	T_M (mV)
Simulation			
S1	55; 70; 85 → 60; 75; 90	23.07	19.26
	60; 75; 90 → 55; 70; 85	22.91	26.22
	55; 70; 85 → 50; 65; 80	29.69	23.00
	50; 65; 80 → 55; 70; 85	23.63	25.93
S2	60; 75; 90 → 65; 80; 95	35.99	29.37
	65; 80; 95 → 60; 75; 90	35.86	35.84
	60; 75; 90 → 55; 70; 85	21.65	29.15
	55; 70; 85 → 60; 75; 90	24.06	21.67
Experiment			
S1	55; 70; 85 → 60; 75; 90	193.52	20.69
	60; 75; 90 → 55; 70; 85	109.16	25.88
	55; 70; 85 → 50; 65; 80	102.84	31.72
	50; 65; 80 → 55; 70; 85	162.39	20.98
S2	60; 75; 90 → 65; 80; 95	149.66	25.61
	65; 80; 95 → 60; 75; 90	229.21	25.61
	60; 75; 90 → 55; 70; 85	110.92	27.09
	55; 70; 85 → 60; 75; 90	183.66	23.16

Table 5
Performance and transient results for Level 3 SST with $\overline{k}=29$ in (8).

Freq. (Hz)	G_A (dB)	D_A (dB)	M_A (dB@Hz)	T_N (10^{-3} V^2)	R_N (10^{-3} V^2)	T_M (mV)	α (–)
Simulation							
50;65;80	36.14	26.43;22.48;27.15	13.35@104.70	79.12	9.07	46.34	1.0391
55;70;85	36.86	29.88;25.15;28.93	11.48@104.70	93.82	8.30	51.86	0.96486
60;75;90	33.81	26.88;22.03;25.06	12.61@112.50	95.94	11.19	55.63	0.97871
65;80;95	29.14	21.76;20.20;14.89	14.16@114.10	97.04	16.10	58.55	0.97945
Experiment							
50;65;80	24.02	27.19;7.84;24.53	21.93@103.10	160.26	47.74	40.99	1.5759
55;70;85	21.64	24.90;7.71;19.79	20.99@103.10	119.40	52.02	43.46	0.80835
60;75;90	13.76	25.91;3.14;19.96	22.76@132.80	164.44	115.66	57.02	1.1032
65;80;95	15.70	23.48;12.11;4.68	24.34@137.50	150.17	82.79	53.28	1.0719

disturbance rejection is caused by the weighting of the control energy during the adaptation, trading off the amount of control energy available for disturbance rejection. A summary of the performance and transient effects for the different Level 3 disturbances is summarized in Tables 5 and 6, indicating smaller disturbance rejection of all three harmonic disturbances, while one of the three harmonic disturbances had limited rejection in the experimental results.

3.7. Conclusions

The weighted Robust Estimation and Automatic Controller Tuning (REACT) uses coprime factorization of a model and an initial controller to create filtered signals from closed-loop measurements. The filtered signals are used to formulate a Recursive Least Squares algorithm to simultaneously minimize the variance of a performance signal and a control signal via the direct estimation of a feedback controller transfer function parametrized in a Youla–Kucera parametrization. The end results are an adaptive regulation algorithm that preserves closed-loop stability and optimizes the trade-off between output and control signal variance. Regularization and filtering of the parameter estimates smoothen the volatility of the recursive parameter updates when the adaptive regulation controller is initialized and/or adjusted to reduce periodic disturbances with sudden jumps in the frequency content. The approach is successfully demonstrated on a vibration control benchmark with harmonic disturbances and excellent results are obtained in terms of performance and transient properties for (multiple) harmonic disturbances in which frequencies change in either a step- or ramp-wise way.

References

[1] B. Anderson, From Youla–Kucera to identification, adaptive and nonlinear control, Automatica 34 (1998) 1485–1506.
[2] M. Bodson, Rejection of periodic disturbances of unknown and time-varying frequency, International Journal of Adaptive Control and Signal Processing 19 (March–April (2–3)) (2005) 67–88.
[3] M. Bodson, Rejection of periodic disturbances of unknown and time-varying frequency, International Journal of Adaptive Control and Signal Processing 19 (March–April (2–3)) (2005) 67–88.
[4] S. Boyd, L. Vandenberghe, Convex Optimization, Cambridge University Press, March 2004.
[5] Y.-Q. Chen, K.L. Moore, J. Yu, T. Zhang, Iterative learning control and repetitive control in hard disk drive industry—a tutorial, International Journal of Adaptive Control and Signal Processing 22 (2007) 325–343.
[6] R.A. de Callafon, J. Zeng, Recursive filter estimation for feedforward noise cancellation with acoustic coupling, Journal of Sound and Vibration 291 (2006) 1061–1079.
[7] S.G. Douma, P.M.J. Van den Hof, O.H. Bosgra, Controller tuning freedom under plant identification uncertainty: double youla beats gap in robust stability, Automatica 39 (2003) 325–333.
[8] C. Du, L. Xie, Modeling and Control of Vibration in Mechanical Systems, CRC Press, 2010.
[9] B.A. Francis, W.M. Wonham, The internal model principle of control theory, Automatica 12 (September (5)) (1976) 457–465.
[10] S. Haykin, Adaptive Filter Theory, Prentice-Hall, Inc., Upper Saddle River, New Jersey 07458, 2002.
[11] P.S. C Heuberger, P.M.J. Van den Hof, B. Wahlberg, Modelling and Identification with Rational Orthogonal Basis Functions, Springer-Verlag, London, 2005.
[12] C. Kinney, H. Fang, R.A. de Callafon, M. Alma, Robust estimation and automatic controller tuning in vibration control of time varying harmonic disturbances, in: Prepr. 18th IFAC World Congress, Milan, Italy, 2011, pp. 5401–5406.
[13] I.D Landau, T.B. Airimitoaie, A. Castellanos Silva, G. Buche, Benchmark on Adaptive Regulation, 2012 ⟨http://www.gipsa-lab.grenoble-inp.fr/∼ioandore.landau/benchmark_adaptive_regulation/⟩.
[14] I.D. Landau, T.B. Airimitoaie, A. Castellanos Silva, G. Buche, Benchmark on adaptive regulation: rejection of unknown/time-varying multiple narrow band disturbances, in: Proceedings of the 12th European Control Conference, Zürich, Switzerland, 2013.
[15] I.D. Landau, A. Constantinescu, M. Alma, Adaptive regulation—rejection of unknown multiple narrow band disturbances, in: Proceedings of the 17th Mediterranean Conference on Control and Automation, Thessaloniki, Greece, 2009, pp. 1056–1065.
[16] I.D. Landau, R. Lozano, M. M'Saad, A. Karimi, Adaptive regulation—rejection of unknown disturbances, Communication and Control Engineering (2011) 477–497.
[17] L. Ljung, System Identification: Theory for the User, second ed., Prentice-Hall, Englewood Cliffs, NJ USA, 1999.
[18] R.W. Longman, Iterative learning control and repetitive control for engineering practice, International Journal of Control 73 (2000) 930–954.
[19] H. Niemann, Dual Youla parameterisation, IEE Proceedings Control Theory Applications 150 (2003) 493–497.
[20] D.S. Ortiz, J.S. Freudenberg, R.H. Middleton, Feedback limitations of linear sampled-data periodic digital control, International Journal of Robust and Nonlinear Control 10 (2000) 729–745.
[21] G. Pipeleers, J. Swevers, B. Demeulenaere, Optimal linear controller design for periodic inputs, in: M. Thoma, F. Allgöwer, M. Morari (Eds.), Lectures Notes in Control and Information Sciences, Springer Verlag, Berlin, Heidelberg, Germany, 2009.
[22] M.M. Seron, J.H. Braslavsky, P.V. Kokotovic, D.Q. Mayne, Feedback limitations in nonlinear systems: from bode integrals to cheap control, IEEE Transactions on Automatic Control 44 (1999) 829–833.
[23] M. Steinbuch, Repetitive control for systems with uncertain period-time, Automatica 38 (12) (2002) 2103–2109.
[24] M. Tomizuka, Dealing with periodic disturbances in controls of mechanical systems, Annual Reviews in Control 32 (2008) 193–199.
[25] M. Tomizuka, T.C. Tsao, K. Chew, Analysis and synthesis of discrete-time repetitive controllers, ASME Journal of Dynamic Systems, Measurement, and Control 111 (September (3)) (1989) 353–358.
[26] P.M.J. Van Den Hof, R.A. de Callafon, Multivariable closed-loop identification: from indirect identification to dual-Youla parametrization, in: Proceedings of the 35th IEEE Conference on Decision and Control, IEEE, Kobe, Japan, 1996, pp. 1397–1402.
[27] K. Zhou, J.C. Doyle, Essentials of Robust Control, Prentice Hall, Upper Saddle River, NJ, 1997.